

## Synthesis of $\text{Li}_3\text{V}_2(\text{PO}_4)_3/\text{C}$ Composites as Cathode Materials for Lithium Ion Batteries via a Sol-Gel Method

Xiaoyu Cao<sup>1,\*</sup>, Hailian Wu<sup>1</sup>, Peng Ge<sup>1</sup>, Yang Zhao<sup>1</sup>, Limin Zhu<sup>1</sup>, Feng Liu<sup>2</sup>, Jufeng Wang<sup>3</sup>

<sup>1</sup> School of Chemistry and Chemical Engineering, Henan University of Technology, Zhengzhou 450001, People's Republic of China

<sup>2</sup> Henan Foodstuffs Import and Export Group-Yude Trading Co., Ltd., Zhengzhou 450001, People's Republic of China

<sup>3</sup> Zhengzhou Zhiqin Science and Technology Co., Ltd., Zhengzhou 450002, People's Republic of China

\*E-mail: [caoxy@haut.edu.cn](mailto:caoxy@haut.edu.cn)

Received: 2 January 2015 / Accepted: 29 January 2015 / Published: 24 February 2015

---

$\text{Li}_3\text{V}_2(\text{PO}_4)_3/\text{C}$  composite cathode materials were successfully synthesized via a sol-gel route based on  $\text{LiOH}\cdot\text{H}_2\text{O}$ ,  $\text{V}_2\text{O}_5$ ,  $\text{NH}_4\text{H}_2\text{PO}_4$  and  $\text{C}_6\text{H}_8\text{O}_7\cdot\text{H}_2\text{O}$  (citric acid) as raw materials. Citric acid acts as a chelating reagent and a carbon source during the synthesis process, which can improve the conductivity of the composite materials and hinder the growth of  $\text{Li}_3\text{V}_2(\text{PO}_4)_3$  particles. The thermal stability, crystal structure and morphology of the as-prepared powders were characterized by thermogravimetric analysis (TG-DTG), X-ray diffraction (XRD), scanning electron microscope (SEM), and transmission electron microscope (TEM). The results indicate that the sintering temperatures have a remarkable effect on the crystal structure, morphology and particle size of  $\text{Li}_3\text{V}_2(\text{PO}_4)_3/\text{C}$  composites. Demonstrated by XRD patterns,  $\text{Li}_3\text{V}_2(\text{PO}_4)_3/\text{C}$  composites have a monoclinic structure indexed to the  $P2_1/n$  space group and well crystallized single phase calcined at 800 °C. TEM images show  $\text{Li}_3\text{V}_2(\text{PO}_4)_3/\text{C}$  particles are roughly nanospheres in the diameter of about 50 nm embedded in carbon networks. Electrochemical tests show that  $\text{Li}_3\text{V}_2(\text{PO}_4)_3/\text{C}$  composite synthesized at 800 °C for 8 h displays the best electrochemical performances among these  $\text{Li}_3\text{V}_2(\text{PO}_4)_3/\text{C}$  composites.  $\text{Li}_3\text{V}_2(\text{PO}_4)_3/\text{C}$  composite synthesized at 800 °C for 8 h shows that the discharge capacities in the first and 100th cycle are 169.65 and 131.72 mAh g<sup>-1</sup>, respectively, in the voltage of 3.0–4.8 V at the current rate of 30 mA g<sup>-1</sup>. When the current rate is raised to 120 mA g<sup>-1</sup>,  $\text{Li}_3\text{V}_2(\text{PO}_4)_3/\text{C}$  composite calcined at 800 °C for 8 h delivers the high initial capacity of 156.04 mAh g<sup>-1</sup> and still maintains a capacity of 123.5 mAh g<sup>-1</sup> after 100 cycles, indicating that  $\text{Li}_3\text{V}_2(\text{PO}_4)_3/\text{C}$  composite with high discharge capacity and good rate capability can be obtained via this sol-gel method.

---

**Keywords:**  $\text{Li}_3\text{V}_2(\text{PO}_4)_3/\text{C}$  composites; Cathode materials; Sol-gel synthesis; Lithium ion batteries; Electrochemical performances

## 1. INTRODUCTION

Lithium ion batteries (LIBs) have attracted much attention for their high energy density, low self-discharge rate, and long cycling life since their commercialization [1]. In recent years, along with the urgent demand for large capacity and high power type LIBs, the development of high-performance cathode materials has become the research focus. Among these known cathode materials, monoclinic  $\text{Li}_3\text{V}_2(\text{PO}_4)_3$  (LVP) is considered as one of promising cathode material candidates. LVP possesses a sodium super ionic conductor (NASICON) structure with the highest theoretical capacity ( $197 \text{ mAh g}^{-1}$ ) in all phosphate cathode materials when three  $\text{Li}^+$  ions are completely extracted [2,3]. Moreover, the 3D framework in the NASICON crystal structure leads to a much higher diffusion coefficient of  $\text{Li}^+$  ion than that in the 1D framework of the olive crystal structure such as  $\text{LiFePO}_4$  [4,5]. However, the polarization of the V-O bonds in LVP leads to a very poor electronic conductivity for pure LVP [6,7]. In order to improve the electrochemical performances of LVP, there are various modified strategies such as doping metal ions into LVP lattice [8–13], and preparing LVP composites including LVP/metal powders [14–15], LVP/carbon [16–21], and LVP/metal oxides [22]. Hereinto, preparation of LVP/carbon composites (LVPCs) and formation of thin carbon coated LVP is the simple and effective way to enhance the electronic conductivity of LVP.

In addition, synthesis and post-processing method which will lead to different microstructures and morphologies for electrode materials have a remarkable effect on electrochemical performances of LVPCs. At present, the traditional solid state synthesis method and the soft chemical synthesis method are the main routes to prepare LVPCs. However, the traditional solid state synthesis method needs high sintering temperature and long sintering time which lead to a wide range of particle size distribution, thereby resulting in low discharge capacity and poor rate capability and hampering its practical application in LIBs. The other is to employ various soft chemical synthesis method such as the sol-gel method [1–3, 18–19], the hydrothermal synthesis method [23–25], the rheological phase reaction method [21, 26–29], the microwave-assisted synthesis method [30–33], and the freeze-drying synthesis method [34]. These soft synthesis reactions are usually carried out under the milder condition due to preparing the homogeneous precursors, which results in the well-developed crystal structure and well-controlled morphological particle at the lower calcination temperature over the shorter dwell time, and accordingly improve the electrochemical performances of LVPCs. Of these soft synthesis methods, the sol-gel method can promote raw materials to reach atomic level mixing, which reduces particle size of the resulting material to micrometer or nanometer level in the subsequent calcination process.

In this work, monoclinic LVPCs were synthesized by a sol-gel method based on citric acid as reducing agent and carbon source, and the resulting electrochemical properties were investigated. Experiment results showed that as-prepared LVPCs displayed high capacity and good cyclic stability.

## 2. EXPERIMENTAL

The monoclinic LVPCs were synthesized by a sol-gel method based on citric acid as chelating agent and reducing agent, and using  $\text{V}_2\text{O}_5$  powder as a vanadium source in this work. Traditionally, the

chelating reagent just only provided the complexing anion at the molecular level during the process of forming sol-gel. But, here citric acid was not only used as a chelating reagent, but also as a carbon source which can prevent the oxidation of vanadium ions and afford the network structure of carbon for enhancing electronic conduction of LVP [16]. All the starting raw materials were the analytical pure reagents and as-received. In the first step, the stoichiometric ratios of  $\text{LiOH}\cdot\text{H}_2\text{O}$ ,  $\text{V}_2\text{O}_5$  and  $\text{NH}_4\text{H}_2\text{PO}_4$  powders were mixed thoroughly by grinding in an agate mortar and then dissolved in the deionized water for ultrasonic treatment. Secondly, a saturated citric acid solution was added dropwise into the mixed solution under magnetic stirring. Afterwards, the mixed solution was mildly heated with continuous stirring to evaporate the excess water at  $80\text{ }^\circ\text{C}$ , and mazarine homogeneous sol became gel. The resulting gel was dried in an air oven at  $100\text{ }^\circ\text{C}$  for 12 h to obtain LVPC precursor. Thirdly, the LVPC precursor was pre-heated at  $350\text{ }^\circ\text{C}$  for 3 h under argon atmosphere in a tube furnace and then cooled to room temperature. Then, the pre-heated material was ground and calcined at different temperatures (600, 700, 750, 800, 850, and  $900\text{ }^\circ\text{C}$ , respectively) for 8 h under argon flow to yield the LVPCs. For the sake of convenience, the six LVPCs were designated as LVPC-1, LVPC-2, LVPC-3, LVPC-4, LVPC-5, and LVPC-6, respectively.

TG-DTG analysis of the LVPC precursor was measured on a Linseis STA PT1600 (Germany) instrument over a temperature range of  $25\text{--}1000\text{ }^\circ\text{C}$  at a heating rate of  $10\text{ }^\circ\text{C min}^{-1}$  under an argon flow. XRD analysis was carried out on a Rigaku D/Max-2500 diffractometer (Rigaku, Japan) with  $\text{Cu K}\alpha$  radiation ( $\lambda = 1.54056\text{ \AA}$ ). The particle size and morphology of the as-synthesized LVPCs were studied by SEM (JSM-6510LV) and TEM (Philips Tecnai G2 20).

To examine the electrochemical performances of resultant LVPCs, galvanostatic charge/discharge cycles were carried out at different current densities over a voltage range of  $3.0\text{--}4.8\text{ V}$  on a multi-channel CT-3008W-5V5mA-S4 battery tester (Shenzhen Neware Electronics Co., Ltd) by using CR2016 type coin cells at  $25\text{ }^\circ\text{C}$ . The cathode films were composed of the as-synthesized active LVPCs powders, super P and polytetrafluoroethylene microemulsion binder (PTFE, 60 wt. %) at a weight ratio of 8:1:1. The working electrodes were fabricated by loading the cutting disc films with a diameter of 1.0 cm into the aluminum meshes, and then they were subjected to a pressure of 20 MPa to fabricate cathode. Lithium foil (Wuhan Newthree Technology Co., Ltd) was served as counter-electrode and the commercial polyethylene (PE) microporous film (ND420 H129-100, Asahi Kasei Chemical Co.) was used as separator. The electrolyte solution was  $1\text{ mol dm}^{-3}\text{ LiPF}_6$  in a mixture of ethylene carbonate (EC) and dimethyl carbonate (DMC) (1:1 by volume, provided by Zhangjiagang Guotai-Huarong New Chemical Materials Co., Ltd). The CR2016 type coin cells were assembled in a high purified argon-filled glove box (JMS-3, Nanjing Jiumen Automation technology Co., Ltd), where the coin cell cases are stainless-steel and purchased from Shenzhen Meisen Machine-electro Equipment Co., Ltd, China. Cyclic voltammetry (CV) was performed on a CHI660D electrochemical workstation (Shanghai Chenhua Crop.) at different scan rates on the potential interval of  $3.0\text{--}4.8\text{ V}$  (*vs.*  $\text{Li}^+/\text{Li}$ ) by using three electrodes system. The electrochemical impedance spectroscopy (EIS) was also

recorded by a CHI660D electrochemical workstation over the frequency range from 100 kHz to 10 mHz with an amplitude of  $\pm 5$  mV.

### 3. RESULTS AND DISCUSSION

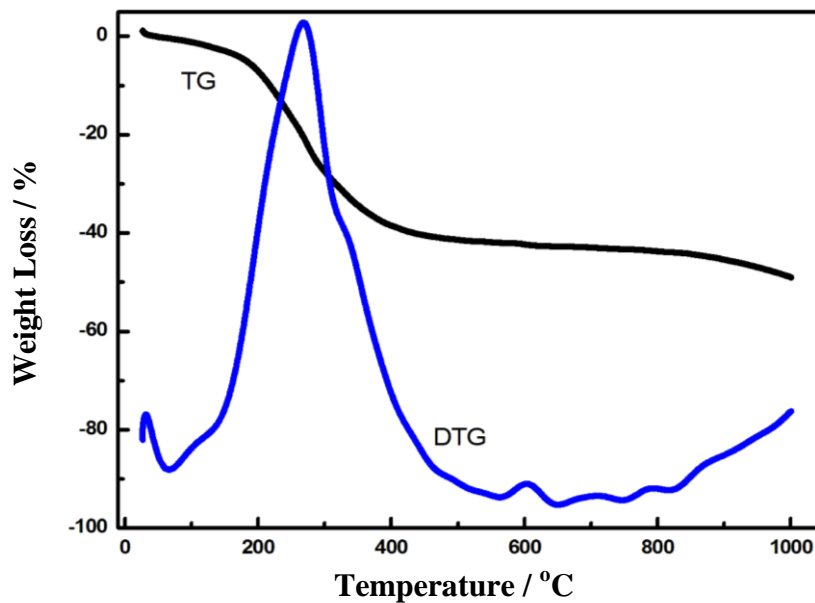


**Figure 1.** TG-DTG curves of LVPC precursor.

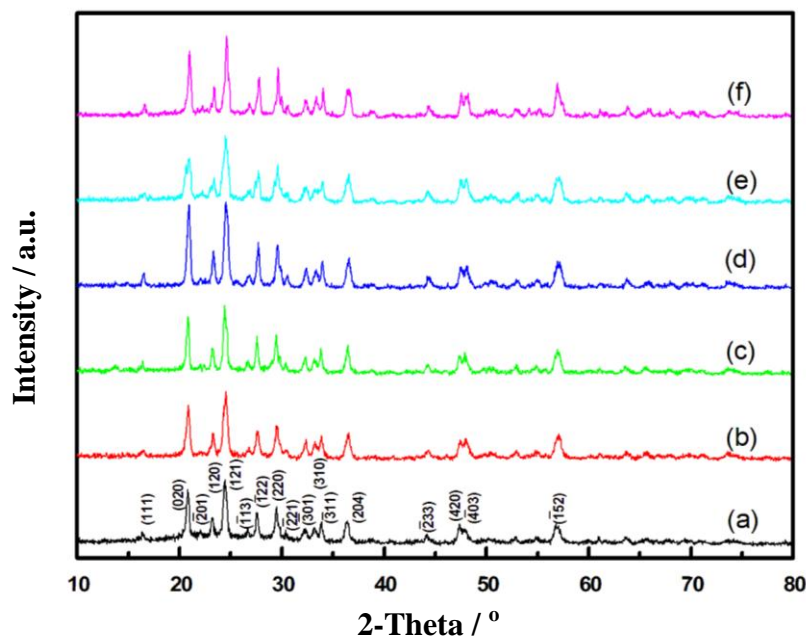


**Figure 2.** XRD patterns of LVPCs calcined at different temperatures for 8 h. (a) LVPC-1, (b) LVPC-2, (c) LVPC-3, (d) LVPC-4, (e) LVPC-5, and (f) LVPC-6.

Fig. 1 is TG-DTG curves of LVPC precursor heated between 25 and 1000 °C under argon flow. TG curve shows three main weight-loss stages. The first one occurred between 25 and 200 °C is attributed to the release of ammonia and liberation of water. The second step of around 32% weight loss which occurs from 200 to 400 °C may be related to the pyrolysis process of citric acid to form oxycarbide and residual carbon. Subsequently, the weight loss between 400 and 600 °C can be ascribed to the reduction of  $V^{5+}$  ions to  $V^{3+}$  ions, the pyrolysis of the remaining citric acid and the formation of crystalline LVPC. From 600 to 900 °C, no weight loss could be observed in the TG curve, indicating the formation of well-crystallized LVPC. Above 900 °C, the weight loss turns evident again, which may be attributed to some side reactions leading to the decomposition of LVPC. Based on this study, we choose the heat-treating temperature which is equal or below 900 °C, which is consistent with the temperature window for carbothermal reduction reaction [35].

XRD patterns of LVPCs synthesized by the sol-gel method at different temperatures are presented in Fig. 2. The crystalline phase of as-prepared LVPCs is similar to the previous report [16]. As shown in Fig. 2, the profiles of the reflection peaks are quite sharp and symmetric. At the same time, the intensities of Bragg diffraction peaks of as-synthesized LiVPCs are heightened with increasing of the calcination temperature. All the characteristics diffraction lines are labeled with miller indices and can be attributed to the monoclinic-phase LVP without presence of any detectable impurities. However, the carbon can not be detected from XRD patterns, which may be ascribed to its amorphous structure or due to that the thickness of the residual carbon on the surface of LVP is too thin [36]. The XRD results herein mentioned indicate that the single phase LVPCs can be successfully obtained through the sol-gel method. The lattice parameters of LVPCs are calculated by means of least-squares method in terms of monoclinic structure with  $P2_1/n$  space group and listed in Table 1.

**Table 1.** The lattice parameters of LVPCs calcined at different temperatures

LVPCs	$a$ (Å)	$b$ (Å)	$c$ (Å)	$\beta$ (°)	$V$ (Å <sup>3</sup> )
LVPC-1	8.5557	8.6282	11.9281	90.4002	880.51
LVPC-2	8.4331	8.6884	12.0375	89.9363	881.99
LVPC-3	8.5417	8.6114	12.0349	89.9398	885.24
LVPC-4	8.4277	8.6886	12.1241	89.9682	887.79
LVPC-5	8.4638	8.6948	12.0328	90.1770	885.51
LVPC-6	8.4650	8.6340	12.1092	89.3948	884.97

As seen in Table 1, the cell volumes of LVPCs first swell and then shrink with the increase of calcination temperature. A maximum cell volume of 887.79 Å<sup>3</sup> is obtained for LVPC-4. According to the previous reports [10, 21, 23], large lattice constants will make  $Li^+$  ions move more freely in LVPC host material. As a consequence, higher capacity and rate capability for LVPC-4 are to follow on.

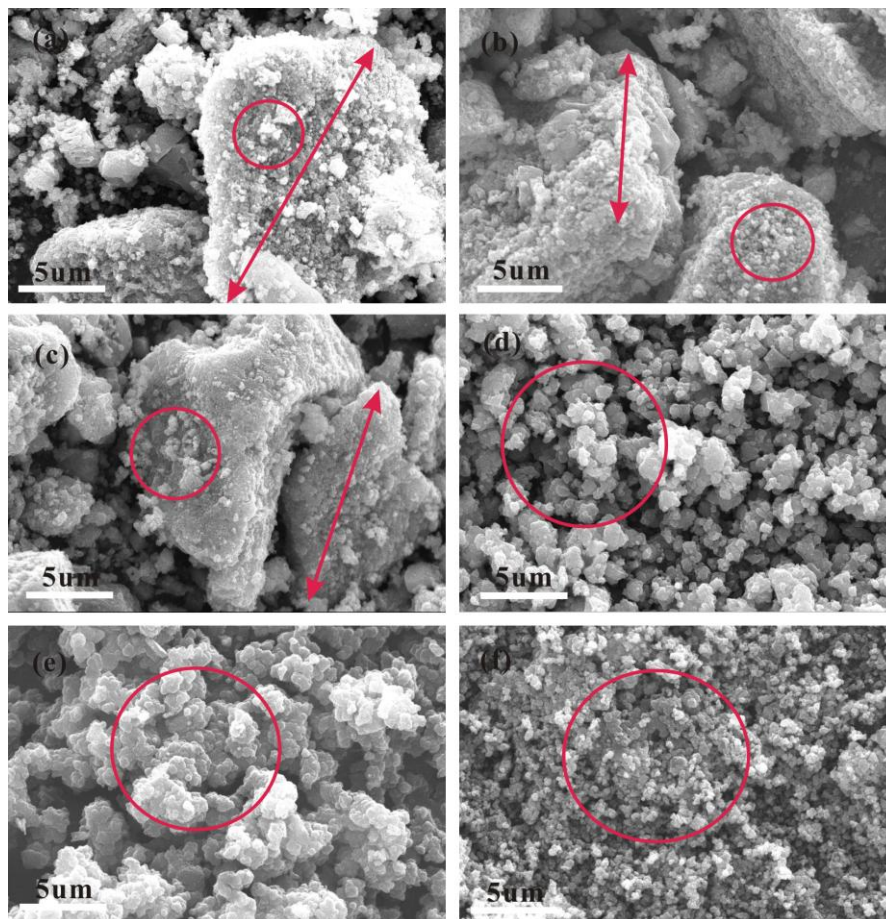


**Figure 3.** SEM images of LVPCs calcined at different temperatures for 8 h. (a) LVPC-1, (b) LVPC-2, (c) LVPC-3, (d) LVPC-4, (e) LVPC-5, and (f) LVPC-6.

SEM images were used to identify the morphology and measure the particle size of LVPCs. Fig. 3 presents that the morphology of as-prepared LVPCs changes with the increase of calcination temperature. In Fig. 3 (a-c), the size of the some small grains is smaller than 1 μm, however, that of the large particles can reach around 25 μm.

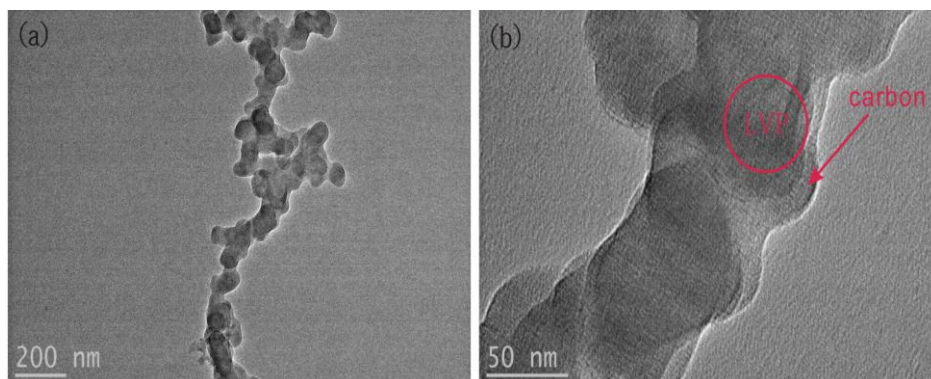


**Figure 4.** TEM images of the LVPC-4.

And it also can be found that the particles of LVPC-1, LVPC-2 and LVPC-3 are seriously agglomerated. Nevertheless, when the calcination temperature is raised to 800 °C, LVPC-4 evolves into small and rather uniform particles reflected in Fig. 3(d), and the average particle size of LVPC-3 is 1 μm, which is advantageous to provide the shorter transport length for the Li<sup>+</sup> ions and electrons diffusion [37]. With the rising of the sintered temperature, the small grains also aggregated together to form a mixture composed of some large secondary particles in Fig. 3(e, f), which would result in lower discharge capacity [2]. To further study the structure of carbon coating layer, TEM was performed on LVPC-4. In Fig. 4 (a), it can be obviously found that LVPC-4 is consisted of roughly spherical particles in the diameter of about 50 nm. The carbon coating layer coming from the decomposition of citric is deposited on the surface of the bare LVP in Fig. 4 (b), and the thickness of the covering layer is around 10 nm, which is very thin and explains why the carbon is not able to be detected in XRD measurement [38].

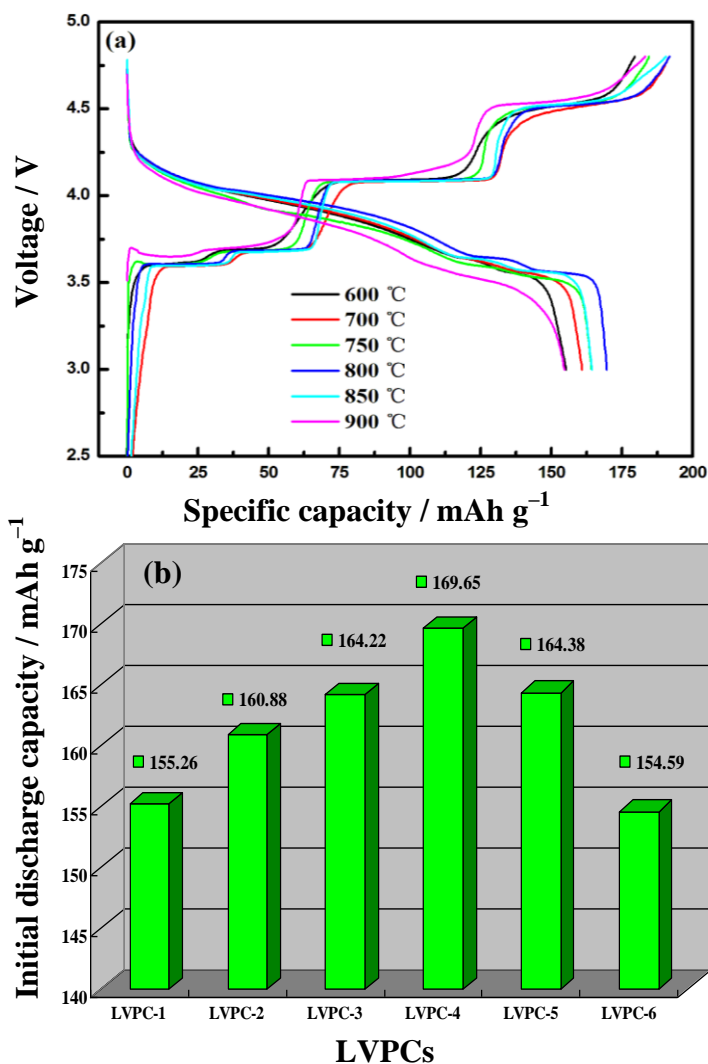


**Figure 5.** The initial charge/discharge curves of LVPCs (a) and bar graphs for initial discharge capacity of LVPCs (b).

Furthermore, the formation of the carbon coating layer not only enhances the electronic conductivity of LVP but also prevent the growth of the LVP grains, which is favorable to improving the electrochemical performances of LVPCs [29].

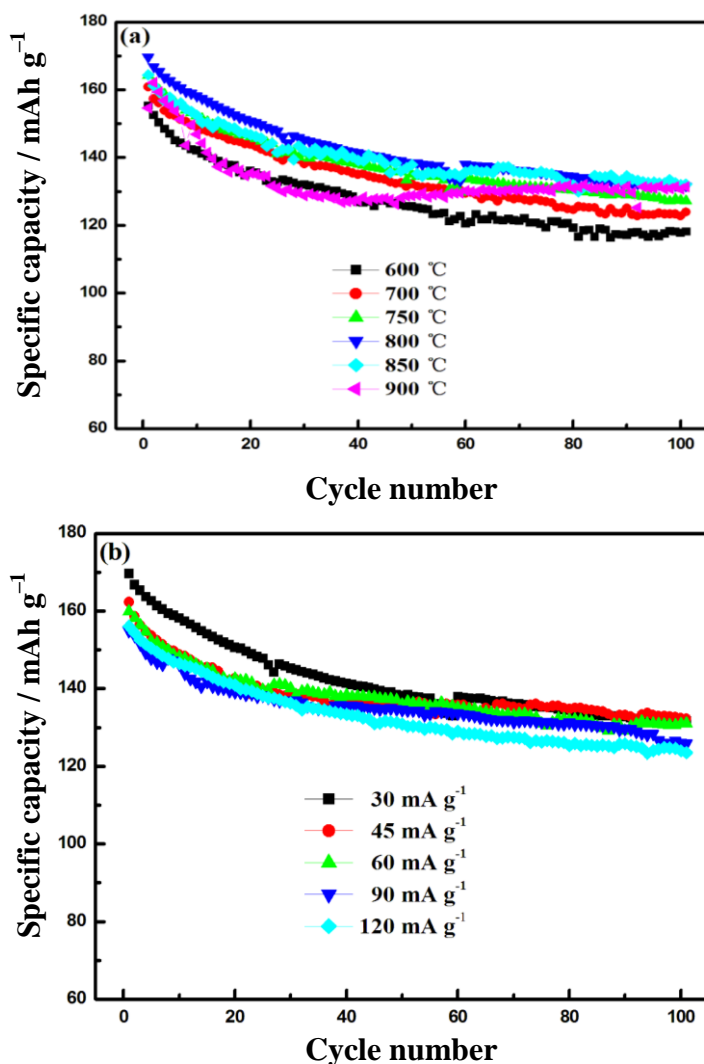


**Figure 6.** The cycling performance of the LVPCs calcined at different temperatures at the current density of 30 mA g<sup>-1</sup> (a), and the cycling performance of LVPC-4 at the different current rates (b).

Fig. 5 presents the initial charge/discharge curves of LVPCs at different sintered temperatures at the current density of 30 mA g<sup>-1</sup> in the voltage range of 3.0–4.8 V. The initial discharge capacities of the different LVPCs are 155.26, 160.88, 164.22, 169.65, 164.38, and 154.59 mAh g<sup>-1</sup>, respectively. In the case of LVPC-4, four charge plateaus at around 3.61, 3.68, 4.09, and 4.52 V correspond to the phase transitions of  $\text{Li}_3\text{V}_2(\text{PO}_4)_3 \rightarrow \text{Li}_{2.5}\text{V}_2(\text{PO}_4)_3$ ,  $\text{Li}_{2.5}\text{V}_2(\text{PO}_4)_3 \rightarrow \text{Li}_2\text{V}_2(\text{PO}_4)_3$ ,  $\text{Li}_2\text{V}_2(\text{PO}_4)_3 \rightarrow \text{LiV}_2(\text{PO}_4)_3$ , and  $\text{LiV}_2(\text{PO}_4)_3 \rightarrow \text{V}_2(\text{PO}_4)_3$  [39]. Among these charge plateaus, plateaus at around 3.61 and 3.68 V arise from the deintercalation of the first Li<sup>+</sup> ion, and plateaus at around 4.09 and 4.52 V originate from the deintercalation of the second and third Li<sup>+</sup> ion. In the discharge process, three plateaus at around 4.01, 3.64, and 3.56 V are related to the reversible intercalation of all three Li<sup>+</sup> ions.

Plateau at around 4.01 V should be ascribed to the intercalation of two  $\text{Li}^+$  ions along with the solid solution behavior, and plateaus at around 3.64 and 3.56 V represent the intercalation of the last  $\text{Li}^+$  ion, demonstrating the two-phase behavior of  $\text{Li}_2\text{V}_2(\text{PO}_4)_3 \rightarrow \text{Li}_{2.5}\text{V}_2(\text{PO}_4)_3 \rightarrow \text{Li}_3\text{V}_2(\text{PO}_4)_3$ . Also, it can be found the discharge platform of LVPC-4 is the highest, which indicates that LVPC-4 would deliver the highest capacity and the maximum energy density. Undoubtedly, high capacity of LVPC-4 should be attributed to its uniform particle size distribution and large cell volume. As aforementioned, the smaller particle size can shorten the diffusion length of  $\text{Li}^+$  ions and electrons, thereby decreasing the electrode polarization. Meanwhile, large cell volume render  $\text{Li}^+$  ions to move more freely in electrode material, which is beneficial for enhancing the electrochemical performances of LVPC-4. However, when the sintered temperature reaches 850 and 900 °C, the initial capacity begins to decrease, which is due to the undesirable agglomerate particles and the adjacency of critical decomposition temperature of LVPC.

The cycling performance of the LVPCs obtained at different sintered temperature is exhibited in Fig. 6 (a) at the current density of  $30 \text{ mA g}^{-1}$  in the voltage range from 3.0 to 4.8 V. After 100 charge/discharge cycles, LVPC-4 can also keep a discharge capacity of  $131.72 \text{ mAh g}^{-1}$ , which is higher than that of the previous reports concerning pristine LVPC [40]. However, LVPC-5 shows a roughly equivalent cyclability after the same cycles compared with LVPC-4, which is related to the second-largest cell volume after LVPC-4. Therefore, the conclusion can be reached that the calcination temperatures have a significant effect on the discharge capacities and cyclic behaviors of LVPCs.

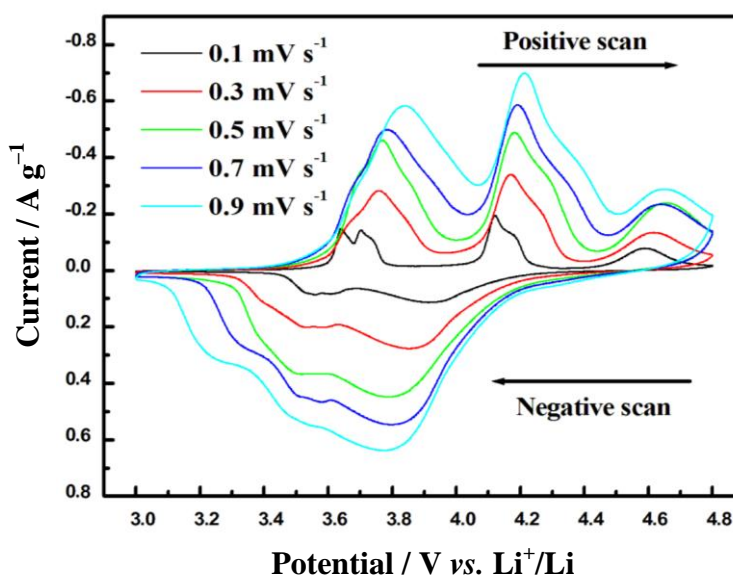


**Figure 7.** CV of as-synthesized LVPC-4 at different scanning rates.

Considering the reduction of energy consumption, LVPC-4 is regarded as the best target product among these LVPCs in this work. The charge/discharge cycling behavior of LVPC-4 was

performed at the different current rates (30, 45, 60, 90, and 120 mA g<sup>-1</sup>, respectively), and the result is presented in Fig. 6 (b). With the increasing of the current density, the discharge capacity of LVPC-4 gradually decreases due to the incompleteness of Li<sup>+</sup> intercalation/deintercalation. However, LVPC-4 displays high initial capacity of 156.04 mAh g<sup>-1</sup> and still maintains a capacity of 123.5 mAh g<sup>-1</sup> after 100 cycles even at the current density of 120 mA g<sup>-1</sup>, exhibiting a good rate capability.

Fig. 7 depicts CV of LVPC-4 at different sweep rates (0.1, 0.3, 0.5, 0.7, and 0.9 mV s<sup>-1</sup>) in the potential window of 3.0–4.8 V. It is all known that CV indicates the oxidation/reduction potential at which Li<sup>+</sup> ions intercalation/deintercalation into/from the lattice as well as phase transitions [41]. During the positive scan, LVPC-4 displays four oxidation peaks at about 3.64, 3.70, 4.12, and 4.59 V at the scan rate of 0.1 mV s<sup>-1</sup>. In the immediate negative scan, there are three reduction peaks at around 3.92, 3.61, and 3.56 V, which is in good agreement with the above galvanostatically charge/discharge platforms in Fig. 5 (a). With the increasing of the scan rate, the shapes of CV have a noticeable change, and the redox peaks at low potential region tend to merge into a single peak, which obviously arises from the intensified electrode polarization. Meanwhile, the currents of anodic and cathodic peaks increase with the aggrandizing of sweep rate, indicating that the redox process of LVPC-4 is a diffusion-limited intercalation process of Li<sup>+</sup> ions [21]. In generally, the speed of Li<sup>+</sup> ions from the bulk electrolyte solution to the surface of porous electrode is more slowly than that of Li<sup>+</sup> ions intercalation reaction when the current rate substantially increases, and Li<sup>+</sup> ions diffusion accordingly becomes the control step for the overall electrochemical reaction.

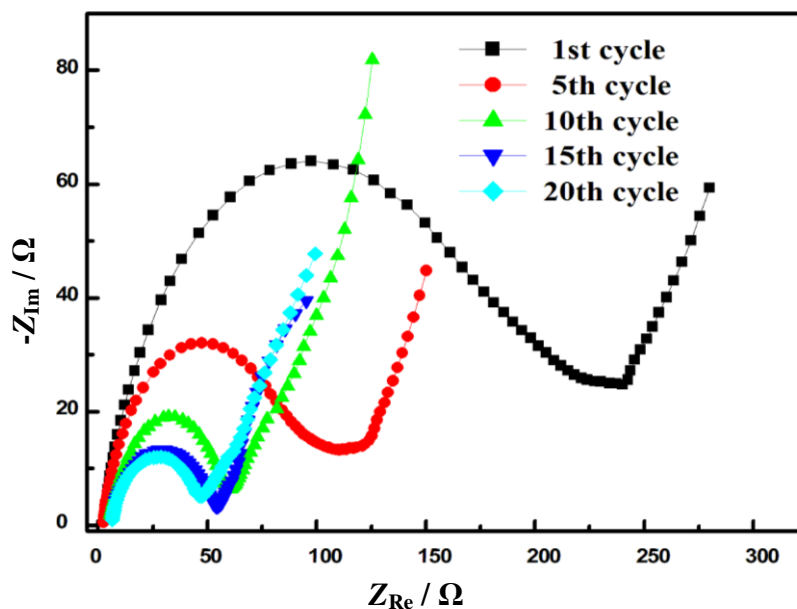


**Figure 8.** EIS of LVPC-4 in the discharged state after different cycles.

In order to further study the electrochemical impedance of the Li<sup>+</sup> ions intercalation/deintercalation process, EIS of the LVPC-4 was performed in the discharged state at the

different cycles and the obtained Nyquist plot is displayed in Fig. 8. It is acknowledged that the impedance of the second battery includes the electrolyte solution resistance ( $R_s$ ), charge-transfer resistance ( $R_{ct}$ ), double-layer capacitance, and the Warburg impedance ( $Z_w$ ). The semicircle curve in the high frequency region is attributed to  $R_{ct}$  between the electrode and electrolyte interface, while the inclined line in the low frequency region represents  $Z_w$ , which is associated with the  $\text{Li}^+$  diffusion in the bulk of solid electrode. It is well known that  $R_{ct}$  is proportional to the diameter of semicircle in the high frequency region and  $Z_w$  is inversely proportional to the slope of the inclined line in the low frequency.

**Table 2.**  $R_{ct}$  simulation values of LVPC-4 electrode at different cycles.

Cycle	1st	5th	10th	15th	20th
$R_{ct}$ ( $\Omega$ )	209.25	100.91	56.67	50.68	42.43

The data of the fitting  $R_{ct}$  is presented in Table 2, and it is found that the  $R_{ct}$  sharply decreases in the first ten cycles. From the 10th cycle, LVPC-4 demonstrates a slight drop in  $R_{ct}$  and an  $R_{ct}$  value of 42.43  $\Omega$  is obtained at the 20th cycle. Because  $R_{ct}$  is the major part of internal resistance of a battery, small impedance is favorable for the  $\text{Li}^+$  ions intercalation/deintercalation during the charge/discharge process, indicating the ability of  $\text{Li}^+$  shuttling between the electrode and electrolyte interface becomes more prominent upon cycling. On the other hand, the inclined line of LVPC-4 in the low frequency region gradually becomes steeper, disclosing that  $\text{Li}^+$  diffusion in LVPC-4 becomes more and more easily. From one side, EIS result supports LVPC-4 synthesized by the sol-gel method to exhibit high discharge capacity and good rate capability.

#### 4. CONCLUSIONS

We have succeeded in preparing of LVPCs by means of the sol-gel method and following heat treatment. The calcination temperature has a significant effect on their crystal structure, morphology and electrochemical behaviors. The as-synthesized LVPCs display high crystallinity without presence of any detectable impurity. SEM and TEM results show that small and homogeneous LVP particles covered by carbon layer with the thickness of around 10 nm can be obtained at 800 °C for 8 h (LVPC-4), which are lower than those of the conventional solid-state reaction. LVPC-4 delivers the first discharge capacity of as high as 169.64 mAh  $\text{g}^{-1}$  and keeps a capacity of 131.72 mAh  $\text{g}^{-1}$  at the 100th cycle with a voltage range of 3.0–4.8 V at the current rate of 30 mA  $\text{g}^{-1}$ . Even operated at the current density of 120 mA  $\text{g}^{-1}$ , LVPC-4 displays high initial capacity of 156.04 mAh  $\text{g}^{-1}$  and still maintains a capacity of 123.5 mAh  $\text{g}^{-1}$  after 100 cycles. High discharge capacity and good rate capability of LVPC-4 should be ascribed to its large cell volume, uniform particle distribution, and good interfacial

compatibility between solid electrode and electrolyte solution. In sum, as-prepared LVPC-4 can be employed as high rate-capability and long-lived cathode material for LIBs.

#### ACKNOWLEDGEMENTS

This work was supported by Innovation Scientists and Technicians Troop Construction Projects of Zhengzhou City, China (Grant No. 131PLJRC652), Program for Henan Science and Technology Open and Cooperation Projects, China (Grant No. 132106000075), Plan for Scientific Innovation Talent of Henan University of Technology, China (Grant No. 2012CXRC09), Key Science and Technology Project of Henan Province, China (Grant No. 122102210114), Science and Technology Project of Jinshui District, Zhengzhou, China (Grant No. 04), Graduate Innovation Fund of Henan University of Technology, China (Grant No. 2012YJXC41), and Zhengzhou Municipal Science and Technology Development Programs, China (Grant No. 112PZDZX019, 20110285).

#### References

1. W. Yuan, J. Yan, Z. Tang, L. Ma, *Ionics* 18 (2012) 329.
2. W. Yuan, J. Yan, Z. Tang, O. Sha, J. Wang, W. Mao, L. Ma, *J. Power Sources* 201 (2012) 301.
3. T. Jiang, W. Pan, J. Wang, X. Bie, F. Du, Y. Wei, C. Wang, G. Chen, *Electrochim. Acta* 55 (2010) 3864.
4. A.K. Padhi, K.S. Nanjundaswamy, C. Masquelier, J.B. Goodenough, *J. Electrochem. Soc.* 144 (1997) 2581.
5. A.K. Padhi, K.S. Nanjundaswamy, B. Goodenough, *J. Electrochem. Soc.* 144 (1997) 1188.
6. S.-C. Yin, H. Grondy, P. Strobel, M. Anne, L.F. Nazar, *J. Am. Chem. Soc.* 125 (2003) 10402.
7. S.-C. Yin, P.S. Strobel, H. Grondy, L.F. Nazar, *Chem. Mater.* 16 (2004) 1456.
8. D. Ai, K. Liu, Z. Lu, M. Zou, D. Zeng, J. Ma, *Electrochim. Acta* 56 (2011) 2823.
9. S.Y. Yang, S. Zhang, B.L. Fu, Q. Wu, F.L. Liu, C. Deng, *J. Solid State Electrochem.* 15 (2011) 2633.
10. S. Zhang, Q. Wu, C. Deng, F.L. Liu, M. Zhang, F.L. Meng, H. Gao, *J. Power Sources* 218 (2012) 56.
11. Q. Kuang, Y. Zhao, X. An, J. Liu, Y. Dong, L. Chen, *Electrochim. Acta* 55 (2010) 1575.
12. C. Dai, Z. Chen, H. Jin, X. Hu, *J. Power Sources* 195 (2010) 5775.
13. L.-L. Zhang, G. Liang, G. Peng, Y.-H. Huang, L. Wang, L. Qie, M.C. Croft, A. Ignatov, J.B. Goodenough, *J. Electrochem. Soc.* 159 (2012) A1573.
14. T. Jiang, Y.J. Wei, W.C. Pan, Z. Li, X. Ming, G. Chen, C.Z. Wang, *J. Alloys Compd.* 488 (2009) L26.
15. L. Zhang, X.L. Wang, J.Y. Xiang, Y. Zhou, S.J. Shi, J.P. Tu, *J. Power Sources* 195 (2010) 5057.
16. Y. Li, Z. Zhou, X. Gao, J. Yan, *Electrochim. Acta* 52 (2007) 4922.
17. J. Wang, J. Liu, G. Yang, X. Zhang, X. Yan, X. Pan, R. Wang, *Electrochim. Acta* 54 (2009) 6451.
18. T. Jiang, W. Pan, J. Wang, X. Bie, F. Du, Y. Wei, C. Wang, G. Chen, *Electrochim. Acta* 55 (2010) 3864.
19. X. Zhou, Y. Liu, Y. Guo, *Electrochim. Acta* 54 (2009) 2253.
20. Y.Q. Qiao, X.L. Wang, J.Y. Xiang, D. Zhang, W.L. Liu, J.P. Tu, *Electrochim. Acta* 56 (2011) 2269.
21. X. Cao, J. Zhang, *Electrochim. Acta* 129 (2014) 305.
22. J. Zhai, M. Zhao, D. Wang, Y. Qiao, *J. Alloys Compd.* 502 (2010) 401.
23. C. Sun, S. Rajasekhara, Y. Dong, J.B. Goodenough, *ACS Appl. Mater. Inter.* 3 (2011) 3772.
24. H. Liu, C. Cheng, X. Huang, J. Li, *Electrochim. Acta* 55 (2010) 8461.
25. C. Chang, J. Xiang, X. Shi, X. Han, L. Yuan, J. Sun, *Electrochim. Acta* 54 (2008) 623.

26. S. Zhong, W. Chen, L. Wu, J. Liu, *Ionics* 18 (2012) 523.
27. J.S. Huang, L. Yang, K.Y. Liu, *Mater. Lett.* 66 (2012) 196.
28. F. Wu, F. Wang, C. Wu, Y. Bai, *J. Alloys Compd.* 513 (2012) 236.
29. C. Chang, J. Xiang, X. Shi, X. Han, L. Yuan, J. Sun, *Electrochim. Acta* 53 (2008) 2232.
30. G. Yang, H. Ji, H. Liu, B. Qian, X. Jiang, *Electrochim. Acta* 55 (2010) 3669.
31. G. Yang, H. Liu, H. Ji, Z. Chen, X. Jiang, *Electrochim. Acta* 55 (2010) 2951.
32. J. Yan, W.-f. Mao, H. Xie, Z.-y. Tang, W. Yuan, X.-c. Chen, Q. Xu, L. Ma, *Mater. Res. Bull.* 47 (2012) 1609.
33. G. Yang, H. Liu, H. Ji, Z. Chen, X. Jiang, *J. Power Sources* 195 (2010) 5374.
34. Y.Q. Qiao, X.L. Wang, Y.J. Mai, X.H. Xia, J. Zhang, C.D. Gu, J.P. Tu, *J. Alloys Compd.* 536 (2012) 132.
35. X.J. Zhu, Y.X. Liu, L.M. Geng, L.B. Chen, *J. Power Sources* 184 (2008) 578.
36. H.C. Shin, W.I. Chob, H. Jang, *J. Power Sources* 159 (2006) 1383.
37. W. Yuan, J. Yan, Z. Tang, O. Sha, J. Wang, W. Mao, L. Ma, *Electrochim. Acta* 72 (2012) 138.
38. L.-L. Zhang, G. Liang, G. Peng, F. Zou, Y.-H. Huang, M.C. Croft, A. Ignatov, *J. Phys. Chem. C* 116 (2012) 12401.
39. X.H. Rui, C. Li, C.H. Chen, *Electrochim. Acta* 54 (2009) 3374.
40. M. Ren, Z. Zhou, Y. Li, X. Gao, P. Yan, *J. Power Sources* 162 (2006) 1357.
41. X.J. Zhu, Y.X. Liu, L.M. Geng, L.B. Chen, *J. Power Sources* 184 (2008) 578.

© 2015 The Authors. Published by ESG ([www.electrochemsci.org](http://www.electrochemsci.org)). This article is an open access article distributed under the terms and conditions of the Creative Commons Attribution license (<http://creativecommons.org/licenses/by/4.0/>).